International Journal of Heat and Mass Transfer 253 (2025) 127543

Contents lists available at ScienceDirect

International Journal of Heat and Mass Transfer

journal homepage: www.elsevier.com/locate/hmt

Experimental investigation of the flow characteristics driving the Ranque–Hilsch phenomenon

Marcel Barzantny [a,*], Mohammed Hussein Hamede [b], Michał Majchrzyk [a], Sebastian Merbold [c], Christoph Egbers [b], Wojciech Kostowski [a]

[a] Silesian University of Technology, Department of Thermal Engineering, Konarskiego 22, 44-100, Gliwice, Poland
[b] Brandenburg University of Technology, Chair of Aerodynamics and Fluid Mechanics, Siemens-Halske-Ring 15a, 03046, Cottbus, Germany
[c] German Aerospace Centre, Institute of Electrified Aero Engines, Lieberoser Straße 13a, 03046, Cottbus, Germany

ARTICLE INFO

Keywords:
Ranque–Hilsch phenomenon
Vortex tube
Flow visualization
Cavitation

ABSTRACT

The Ranque–Hilsch vortex tube (RHVT) is a device that separates a pressurized inlet stream into two decompressed streams of different temperature, flowing to the so-called hot and cold outlets. In this study, the flow structures within the vortex tube were examined qualitatively. The examination considered both compressible and incompressible fluids, using pressurized air and water as working fluids. A parametric study was conducted, in which the fluid inlet pressure and the vortex tube length were varied. Three tubes, with the same diameter but differing lengths (100, 180, and 240 mm) were utilized. The flow inside the tube was investigated using a flow visualization technique, which was employed in a variety of configurations and setups contingent on the specific fluid conditions under examination. The visualization process required the use of aerosol injection in the case of air, and kalliroscope particles in the case of water investigation. The research enabled the visualization of the flow structure within the vortex tube, thereby significantly advancing the comprehension of the underlying physical processes. The findings of the experimental research demonstrated the existence of phenomena of considerable scientific value. The internal vortex and its spatial and temporal structure observed in the RHVT were consistent with literature data. This was achieved despite the so-far established consensus that this type of research is challenging and not entirely reliable. In the course of water-based investigation, the cavitation phenomenon was observed in the vicinity of the internal vortex. This discovery is likely to be the first of its kind and may contribute significantly to the advancement of research on the Ranque–Hilsch phenomenon.

1. Introduction

1.1. The Ranque–Hilsch Vortex Tube - RHVT

The Ranque–Hilsch phenomenon was first discovered in the 1930s [1]. The utilization of a vortex tube facilitates the separation of an inlet mass flux of a specified thermal state into two distinct streams. One of these streams is subjected to an increase in thermal state, while the other is subjected to a decrease in thermal state relative to the initial condition.

Despite the considerable time that has elapsed since then, and the numerous published studies and proposed theories explaining the Ranque–Hilsch effect, no agreement on the root cause has been reached. Previous visualization experiments have not provided a definitive answer to the fundamental question: What the flow structure looks like, how is it formed and how does it work? The vortex tube is a relatively simple device, consisting of four principal elements (Fig. 1): inlet nozzles (1) directed tangentially to the vortex chamber (2), a cone-shaped control valve (3), adjusting the flow rate of hot medium exiting the tube (referred to as the 'hot outlet'), and an orifice (4), allowing the cold stream to exit the chamber at the opposite side (referred to as the 'cold outlet'). The increased pressure of the inlet stream generates high speed and strong swirling flow in the nozzles. As a result of complex thermodynamic processes, an increase and a decrease in temperature are observed at the hot and the cold outlets, respectively. While the application of the vortex tube in refrigeration cycles is under development [2], the identification of physical phenomena responsible for the effect still remains a challenging research issue, although current CFD techniques can accurately predict temperature separation even at steady state with time-averaged flow fields [3]. There are six main hypotheses describing the Ranque–Hilsch phenomenon.

* Corresponding author.
E-mail address: marcel.barzantny@polsl.pl (M. Barzantny).

https://doi.org/10.1016/j.ijheatmasstransfer.2025.127543
Received 27 March 2025; Received in revised form 13 June 2025; Accepted 14 July 2025
Available online 29 July 2025

Nomenclature

Latin symbols

$\dot{m}$	Mass flow rate, kg/s
A	Cross section field, mm^2
c_p	Thermal capacity, J/(g K)
D	Inner diameter, m
h	Specific enthalpy, J/kg
I	Light intensity, –
L	Length, m
p	Pressure, Pa
R	Gas constant, J/(kg K)
r	Radius, m
Re	Reynolds number, –
S	Surface, m^2
T	Gas temperature, K
U	Voltage, V
v	Flow velocity, m/s

Greek symbols

κ	Isentropic exponent, –
ω	Angular velocity, rad/s
τ	Time, s
θ	Tangential direction, –
ϱ	Density, kg/m^3

Shortcuts

CFD	Computational Fluid Dynamics
PIV	Particle Image Velocimetry
R-H	Ranque–Hilsch
RHVT	Ranque–Hilsch Vortex Tube
VT	Vortex Tube

Indexes

c	Cold outlet, –
h	Hot outlet, –
in	Inlet, –

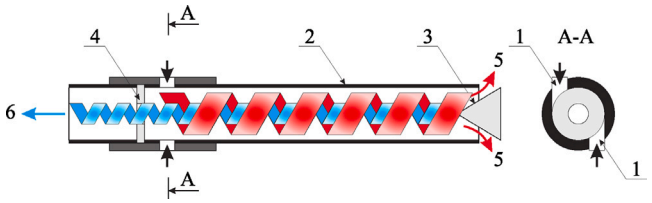

Fig. 1. Vortex Tube construction and hypothetical flow structure [11]. 1 — inlet nozzles, 2 — vortex chamber (tube), 3 — cone shaped control valve, 4 — outlet nozzle(orifice), 5 — hot outlet, 6 — cold outlet.

1.2. Hypothesis overview

Local compression and expansion

While Ranque himself proposed that expansion of the working medium is the inherent cause of temperature reduction [1], the question remains whether the flow also experiences local compression responsible for the increment of temperature. Numerical analyses largely suggest the presence of a radial static pressure gradient [4–7]. Research conducted by Amanti et al. [8] on a vortex tube with the hitherto largest investigated diameter (800 mm) indicates that the compressibility and radial compression of the medium play a pivotal role in temperature rise. However, the influence of local fluid compression on the temperature increment is contested by studies utilizing incompressible media, in which the energy stratification was also observed [9,10].

Secondary circulation and multi-circulation

Despite its strong association with local compression/expansion, the secondary flow is proposed as a distinct mechanism [12,13]. This recirculating flow occurs between the low pressure region in the core and the pressurized region closer to the device walls [14–17], thereby enforcing a local fluid compression and expansion. Schultz-Grunow [18] suggested that turbulence may induce oscillating movements in the stratified centrifugal force field, creating multiple small-scale Joule refrigeration cycles occurring inside the tube.

Göertler vortices

Following other investigations, Stephan et al. [19] propose the existence of Görtler vortices as an independent mechanism underlying the effect. This so-called Görtler instability is characterized by the fluid's radial flow (along the pressure gradient), facilitating localized fluid compression and expansion. The underlying geometry is intricate, further complicating the explanation of this hypothesis.

Surface and internal friction

The R-H effect can also be attributed to both surface and internal fluid friction. Arjomandi et al. [17] and Xue et al. [13], employing an analytical approach, demonstrated that surface friction contributes to a temperature rise of no more than 2 K, indicating its limited influence on the effect. Webster et al. [20] postulated the conversion of the fluid's kinetic energy into heat due to internal friction between the core fluid and the upper layer fluid, rotating with a higher angular velocity. This theory has been corroborated by experimental and numerical studies [21–25]. Hamoudi et al. [26] investigated the air flow in a vortex tube with a 2 mm inner diameter, enabling laminar air flow at the device's inlet, and concluded that the Ranque–Hilsch effect is stronger under turbulent flow conditions, highlighting the significant role of fluid friction. Bej and Sinhamahapatra [27] stated that the R-H effect occurs mostly due to the transfer of *shear work* done by the rotating fluid transferred to the outer zones.

Radial temperature gradient

The radial temperature gradient hypothesis, as initially proposed by Rudolph Hilsch [28] and further developed by Behera et al. [29], suggests that the fluid temperature decreases slightly with the radius of the vortex tube due to the higher fluid velocity in the surface layer. This has the effect of a driving force for heat transfer. However, several studies have challenged this hypothesis, demonstrating that the temperature actually increases with the vortex tube's radius, potentially hindering the Ranque–Hilsch effect [17,23,30–32].

The acoustic effect

Kurosaka [33] postulated the acoustic effect as a primary mechanism underlying the R-H effect. His experiment, later confirmed by Chu [34], involved lining the inner surface of a vortex tube with an acoustic damping material specifically tuned to a particular sound wave frequency. As the flow rate through the device increased (along with the increasing inlet pressure), the sound intensity was rising, and a sudden temperature increase was observed upon reaching the damped sound wave frequency.

Behera et al. [29] conducted a numerical analysis based on the Kurosaka experiment [33], disregarding the acoustic effect. The analysis yielded temperatures at both outlets that were close to the experimentally observed values. These findings suggest a rather secondary influence of flow acoustics on the Ranque–Hilsch effect, however, a thorough research on this hypothesis is still needed.

1.3. Gap in the literature

As shown in the overview of hypotheses, flow processes are complex and still require a more detailed explanation. Understanding the internal processes can substantially be improved by applying a numerical, or preferably, experimental techniques of flow visualization.

Numerical investigation, specifically computational fluid dynamics (CFD), represents the most common approach. Kaufmann developed a model to visualize the flow structure in a counter-flow vortex tube, though it lacked experimental validation [35]. Syed & Renganathan [36] performed a visualization study showing streamlines and vortices within the vortex tube with the use of k-ϵ turbulence model and steady state conditions. However, this model also lacked a correlation with experimental data. Rafiee & Sadeghiazad [37] validated a numerical model with experimental data achieving a maximum discrepancy between CFD model and experimental data of 6.1%. Additionally, they demonstrated the streamlines of internal flow. Different study in steady state conditions was carried out by Gue et al. [38]. A correlation between RHVT performance and internal flow structure due to the vortex tube geometry, i.e. the cold orifice area ratio was investigated. The authors reported significant changes in the reverse flow structure and corresponding averaged temperature flow fields. Another optimization study was performed by Shaji et al. [39] reporting total pressure and temperature distributions in consecutive axial locations with the use of RNG k-ϵ model in steady state simulation. Latest numerical study conducted by Wang et al. [3] on influence of nozzles diameter on RHVT performance showed a significant correlation of nozzles diameter with internal reverse flow and its radius. It was stated, that the optimal performance conditions are obtained when the reverse flow radius and the cold end aperture are matched. Otherwise, according to the authors, the secondary circulation flow may appear and deteriorate the thermal effect, which is in contradiction to the hypothesis of secondary flow. CFD is a powerful tool for potential optimization and better understanding of the Ranque–Hilsch phenomenon. However, it should be used with caution, as published studies often lack experimental validation and the studies themselves are conducted using simpler turbulence models in steady state conditions, which can lead to misleading information about flow structure and behaviour, as the Ranque–Hilsch effect is transient in nature and should be validated regarding the flow structure.

Experimental visualization of fluid flow is rarely found in the literature due to the high flow velocities, complex vortex flow structure and tubular geometry of the separation chamber. The first attempt to visualize flow was made with the use of dye injection by MacGee [40]. Later on Baker used starch as an additive to their air operating vortex tube and reported location of the stagnation point by measuring the wall temperature with thermocouples [41]. A transparent vortex tube and different additives were used by Lay [42] failing to capture flow fields with sawdust and confetti, but the use of coloured liquid showed relatively clear 3D image captured with high speed camera. Different approach was tested by Sibulkin with a mixture of carbon powder and oil [43], while Arbuzov et al. [44] created a dedicated system using the Hilbert visualization technique. The outcome of the experiment was a footage of a vortical double helix. The spiral path of the peripheral flow was also visualized with the use of smoke by Aydin & Baki [45]. In another water investigation with dye injection Li et al. [46] observed counter rotating longitudinal vortex pairs, but experiment was conducted for unrealistically low Reynolds number up to 3500. Xue et al. [47] prepared a system working with water with hydrogen bubble injection. In effect, a rotational axis of the flow was recorded. Additionally, it was possible to track a particle moving from the cold to the hot end. In another approach, Xue et al. [48] used PIV (Particle Image Velocimetry) to visualize the flow with focus on the inner vortex. As a result, the velocity profile was identified and the movement of the vortex core was observed, in agreement with most numerical results. Similar study, but with air-operating vortex tube and LDV measurement technique was performed by Guo et al. [49] obtaining time–averaged axial and radial velocity fields at different axial locations. It was found, that radial velocities are irregular under different cold mass fraction and the stagnation point is not a permanent flow feature needed for heating effect to occur. Shi et al. [50] used 2-D particle image velocimetry (PIV) to investigate the large-scale flow structure and energy separation mechanism within Ranque–Hilsch vortex tubes. The research focused on understanding the roles of unsteady vortex breakdown, precessing vortex cores, and reverse flow boundaries under various operating conditions.

Vortex tube flow visualization requires further research for the following reasons: (i) The reported research was primarily conducted using water. Gas flow visualization sets a significant challenge in experimental research due to the high linear and rotational velocity achieved by the compressible gas medium. Therefore, the use of larger vortex tubes may be necessary to reduce the flow velocity, which limits the parameter range of the reported research. (ii) The experiments revealed that the visualization techniques employed were inadequate in providing a comprehensive understanding of the flow structure. The utilization of low spatial and temporal resolutions has a detrimental effect on the quality of the footage obtained through the PIV or the Hilbert method. (iii) The manufacturing process of transparent vortex tube using acrylic glass frequently leads to artefacts (scratches etc.) deteriorating the visualization quality. (iv) The prevailing focus on numerical simulations entails a relatively poor experimental validation of most numerical results. Most models are only validated by boundary pressure and flow measurements rather than direct flow visualization. As a result, the credibility of the reported research is frequently questionable as the flow pattern formation is not elaborated in detail while quantitative measurements in general rely on assumptions on coherent and time variant flow structures. Thus, flow visualization is essential for the development and validation of high-quality numerical models and the understanding of the nature of the fluid flow.

In this paper, we investigate the flow structure occurring inside the RHVT. The study considers two working fluids: air and water, with inlet parameters of up to: 0,2 bar(g) – air; 2,2 bar(g) – water. One of the objectives of this study is to demonstrate the potential for flow visualization in the RHVT using air as the working fluid and to emphasize the parallels with the case of using water as the working fluid. This objective is achieved by means of aerosol injection in the first medium and kalliroscope particles in the second, which are illuminated by a laser and recorded by a high-speed camera. The observed flow properties and phenomena are then compared to literature data. Based on these, two working principle hypotheses are formulated. Furthermore, unexpected cavitation in the vortex tube was observed and described, presenting novel scientific value in the context of the study.

2. Experimental setup

The construction of the test rig with the vortex tube as the key element had previously been evaluated at an earlier stage of the ATHLETE research project [51]. To adapt the setup for flow visualization, a transparent vortex tube was crafted from acrylic glass, however, some modifications in the nozzle configuration were done compared to the initial experiments. The designed RHVT is illustrated in Fig. 2. The new nozzle element was equipped with 4 nozzles, each of them with 1,5 mm^2 cross-section area. Three tube lengths of 100, 180 and 240 mm were prepared and used in experiments. The lengths were selected based on a review of the literature in relation to the L/D ratio [52]. More information on the geometry and dimensioning of the designed vortex tube is given in Table 1. It was hypothesized that an increase in the length of the tube would lead to an increase in the instability of the phenomenon, which was to be evaluated during the course of this investigation.

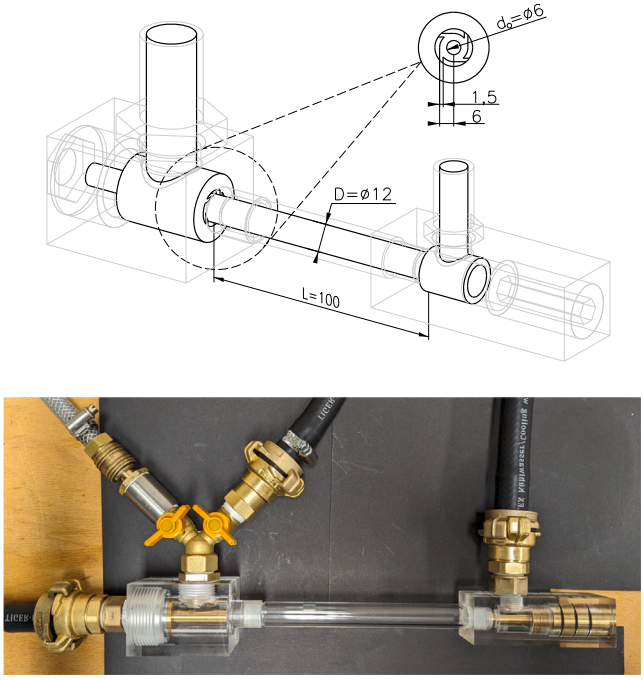

Fig. 2. The vortex tube used for the study. ISO projection, cross-section, and the device prepared for operation.

Table 1
Dimensions of the constructed vortex tube.

Parameter	Value
Vortex tube diameter, mm	12
Outlet orifice diameter, mm	6
Number of nozzles, –	4
Cross-section of single nozzle, mm^2	1,5
Mixing chamber length, mm	100, 180, 240
Cone angle, deg	30
Valve lift on thread, mm per turn	1

2.1. Flow investigation method

The objective of the underlying study is to elucidate the flow pattern and the vortex structure within the RHVT through experimental investigation, thereby advancing the fundamental understanding of the physical processes occurring within the RHVT. It was expected that the findings of this investigation would reveal the flow structure and may provide evidence supporting or denying of the six working hypotheses previously mentioned. To achieve this goal, it was decided to employ a quantitative flow measurement technique, specifically the flow visualization technique.

Fig. 3 depicts a schematic representation of the experimental apparatus, illustrating the various instruments and components utilized for the flow visualization. The configuration of the setup presented was employed throughout the various stages of the investigation. The flow was seeded with specific visualization particles pertinent to the investigated medium. A laser sheet was illuminated within the designated investigation area, and a camera was positioned in a facing orientation relative to the laser sheet. This configuration enabled the capture of the varying flow dynamics through the observation of the illumination emanating from the seeded visualization particles, which are presumed to adhere to the flow patterns. To capture the flow dynamic with high temporal resolution, a high-speed Phantom VEO-640L camera (2560 × 1440 resolution) was utilized. A 100 mm/3.1 macro lens was used with the camera. The illumination of the flow was achieved through the utilization of a green Dantec Dynamics RayPower 450 laser device, operating at a power output of 450 mW and a wavelength of 532 nm. The test rig was constructed over an aluminium profiles setup, which were covered in black cardboard for safety reasons and to minimize the occurrence of unnecessary laser reflections. In the course of this study, two distinct fluids were employed: air and water. The visualization of the flow on each of these two media was conducted in accordance with the procedures outlined below.

2.1.1. Flow visualization with air as a working fluid

In the case of the air-based research, the flow was seeded with aerosol particles via an ATM 230 aerosol generator. This device is working as a two-steam nozzle. Di-Ethyl-Hexyl-Sebacate (DEHS) was used as the operating medium, generating polydisperse aerosol mainly below 1 μm. However, this approach necessitated the utilization of air as the working medium, which, as previously stated, could potentially pose a significant challenge. The experimental facility was designed to accommodate pressures up to 6 bar (g). However, in the present study, the connection of the aerosol to the air inlet, as illustrated in Fig. 3, resulted in a limitation of the inlet pressure. A further series of experiments was conducted to determine the extent of pressure loss that occurs when the aerosol generator is connected between the air compressor and the vortex tube inlet. Fig. 4 shows how significantly the pressure drops when the aerosol generator is connected to the vortex tube inlet, where the maximum inlet pressure achieved is 0.2 bar(g) in this case. Thus, the study is conducted on the verge of occurrence of the phenomenon. To further substantiate the occurrence of the Ranque–Hilsch effect at such low pressures and with aerosol injection into the stream, additional temperature measurements were conducted at both the cold and hot ends. Consequently, it was confirmed that a temperature difference is observable starting from an inlet pressure of 0.01 bar(g). Over the investigated pressure range, this temperature difference varied depending on the tube length: (i) 100 mm tube - 0.01 to 3 °C, (ii) 180 mm tube - 0.01 to 4 °C, and (iii) 240 mm tube - 0.01 to 5.1 °C. Precise data and detailed procedure of the flow visualization within the air medium is presented by Barzantny et al. [53]

2.1.2. Flow visualization with water as a working fluid

In the case of water-based research, the flow was seeded with Kalliroscope particles, such a particle based visualization method is widely used in fluids [54,55]. Kalliroscope particles (or *guanine flakes*) have a typical size of 30 × 6 × 0.07 μm, resulting in a very low Stokes number of $St \approx 8.33 \times 10^{-5}$, assuming a maximum flow velocity of 1 m/s. The low Stokes number of the particles is an indication that the particles presumably follow the flow with an almost negligible sedimentation velocity. The elongated, flat shape of the particles enables them to align with the local shear stress and to reflect light, as demonstrated by [56]. In the case of the long side being oriented towards the observer, the greatest amount of light is reflected. Areas where the particles align in a way that the sharp edge points towards the observer result in a darker zone. The volume fraction of Kalliroscope in comparison to the working fluid is maintained at a level below 10^{-4}. As illustrated in Fig. 3, the flow was mixed with the Kalliroscope particles in an external water reservoir prior to being pumped to the vortex tube. In contrast to the air, the water circulation was maintained in a closed loop to ensure the sustained mixing of the water with the Kalliroscope particles. A mixing pump was continuously operational within the water tank, facilitating regular mixing of water from both the hot and cold outlets of the RHVT. This mixture was then pumped back to the input tank. One might posit that the temperature of the input fluid to the RHVT is subject to variation over time due to the mixing of the outlet fluids with the retained fluid in the tank. However, given that the output volume of fluid compared to the initial volume recovered in the tank (12 l) is insignificant, we have elected to maintain the temperature of the inlet fluid at a constant level throughout the course of the investigation. All pipes and connectors were hermetically sealed with specific sealing materials to prevent any leakage. The primary

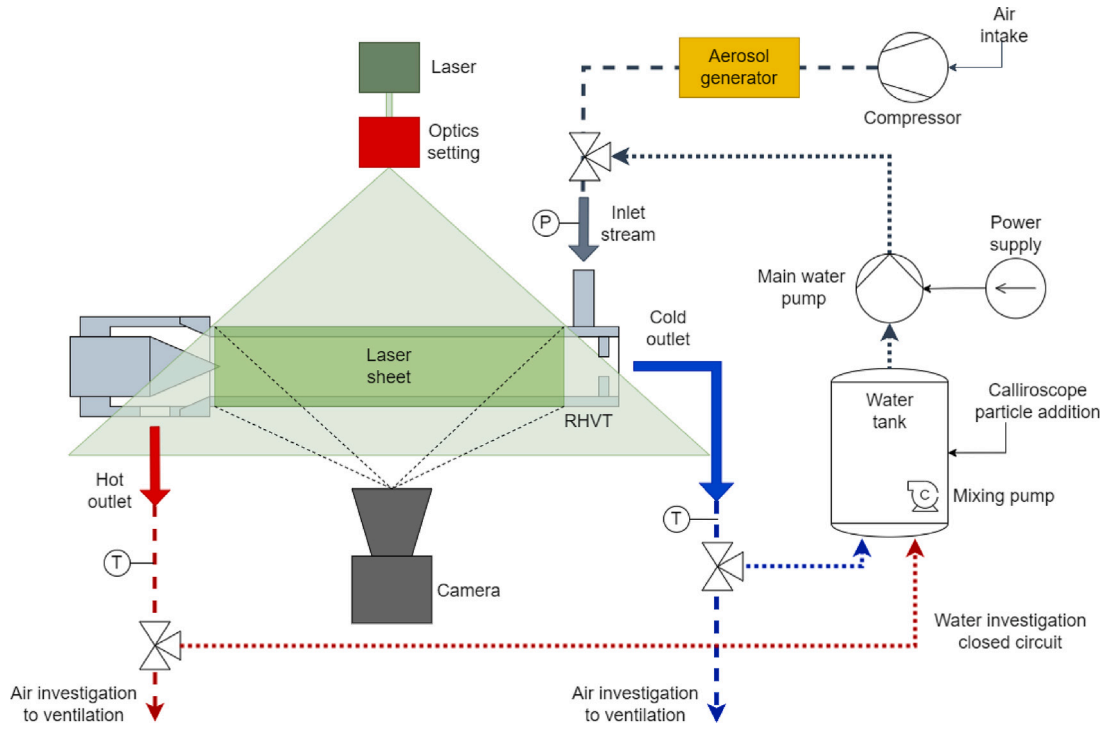

Fig. 3. Schematic of the experimental setup. (For interpretation of the references to colour in this figure legend, the reader is referred to the web version of this article.)

circulating pump was selected based on an analysis of the literature, which indicated that optimal visualization results are achieved for flow in the inlet nozzles when Reynolds numbers reach 10^4 [47]. To improve the description of the observed flow in the context of water, additional measurements of the inlet pressure to the RHVT were conducted. In this instance, the measurement was based on a voltage reading from the pump's power supply and a measurement of the inlet pressure (gauge) to the RHVT, which was made with a pressure transducer. The obtained function for the RHVT inlet pressure is:

$$p = 4.624 \cdot 10^{-5}U^4 - 1.725 \cdot 10^{-3}U^3 + 2.483 \cdot 10^{-2}U^2 + 1.341 \cdot 10^{-2}U - 4.014 \cdot 10^{-4} \quad (1)$$

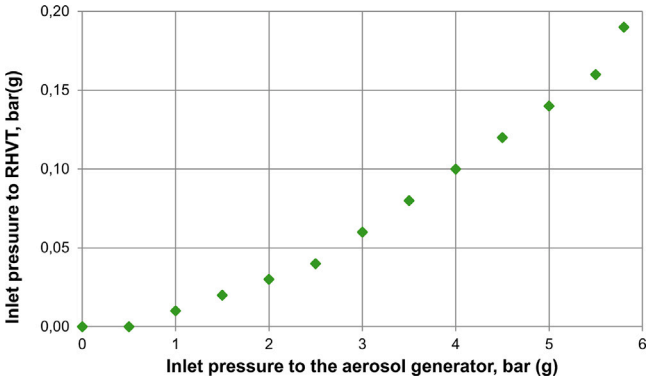

Fig. 4. RHVT inlet pressure determination, related to the pressure drop caused by the aerosol generator.

3. Results

3.1. Air investigation

Two distinct procedures for conducting experiments have been delineated. Firstly, the pressure was gradually increased and the formation of the internal vortex was observed. Secondly, separate recordings were made for seven pressure settings, ranging from 0 to 0.1 bar (g). This allowed the team to observe the flow structure inside the RHVT depending on the inlet pressure and the length of the pipe. Due to the exceedingly high velocities present in the RHVT, even at relatively low pressures, it was not possible to directly observe individual aerosol particles, however, as shown in Fig. 5:

(i) The external flow is observed as a lighter aerosol layer.
(ii) The inner flow can be observed as a darker area without aerosol particles (or with a very small amount concentrated at the boundary of the two pre-flows) inside the outer flow.

With the increase of pressure, the boundary between both flow layers becomes more pronounced, as shown in Fig. 5, presenting the average light intensity value of each pixel in the recorded data set. The graphs indicate that the internal vortex consistently originates from the control valve (hot outlet, left side of every image) and progresses towards the orifice (cold outlet, right side of every image). In the vicinity of the outlet orifice a notable increase in the mixing of the fluid is observed.

The average light intensity I has been defined as:

$$\overline{I} = \frac{1}{\tau_1 - \tau_0} \int_{\tau_0}^{\tau_1} I(\tau) \mathrm{d}\tau, \quad (2)$$

where τ is the time ranging from 0 to 10 s and I is the light intensity obtained as a digital value from the acquisition system, ranging from 0 to 65 535.

3.1.1. Behaviour of the inner core

The term 'behaviour' refers to space- and time variability of the inner core, which is of particular interest for this study and appears to have a novel scientific value. As reported in the Introduction, the research of Xue et al. [47] led to the visualization of the rotational axis of the internal core. The visualization indicated a deviation of the rotational axis from the symmetry axis of the tube. In the course of their

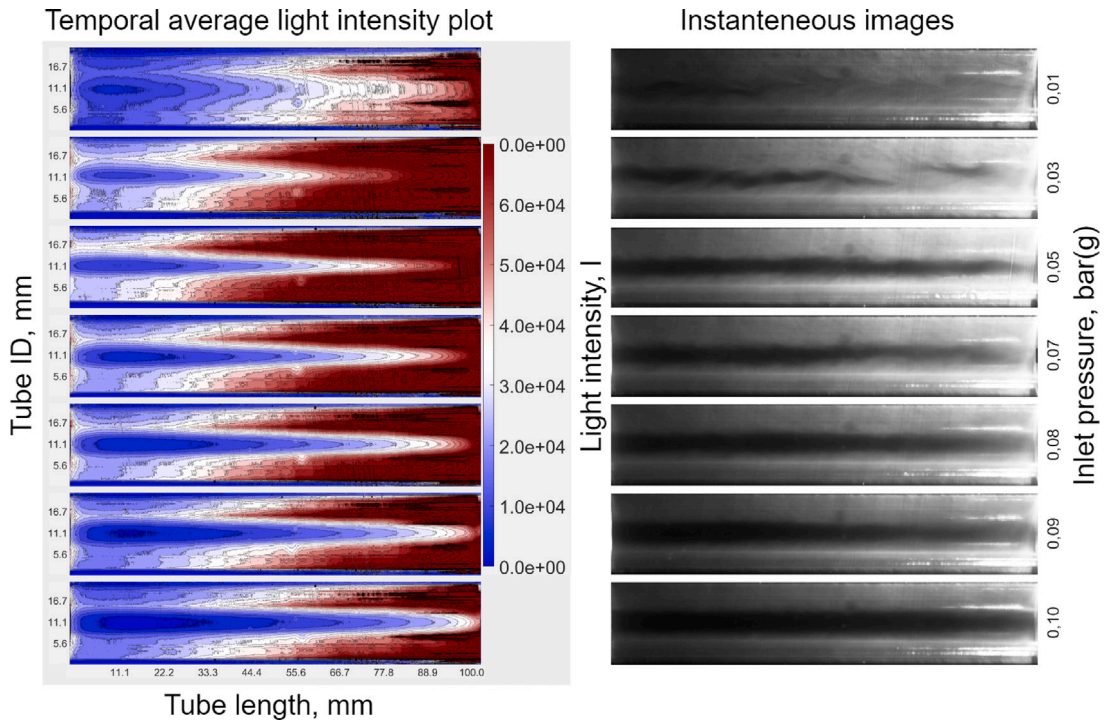

Fig. 5. Left: Counter plots of the temporal average light intensity value between $\tau = 0$ to 10 s. Right: instantaneous images of the 100 mm tube, $\tau = 10$ s.

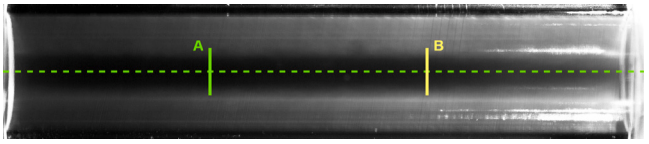

Fig. 6. Instantaneous image of the flow visualization in the RHVT, 100 mm tube, 0,1 bar(g). Marked axis of symmetry (green dotted line) and locations for further post processing: green - A and yellow - B.

research, this observation was made using an experimental setup in which water was used, and the visualization method was based on the injection of hydrogen bubbles into the flow. Additionally, difficulties in repeating such behaviour with the use of air were also identified.

This study demonstrates that air exhibits similar behaviour to water, hence, the rotational axis of the internal core deviates from the axis of symmetry of the pipe as shown in Fig. 6.

These observations were made for each tube length. In the case of a 100 mm tube, the displacement is already visible. For the 180 mm pipe, it is significant, similarly for the 240 mm pipe. This phenomenon is best observed for inlet pressure above 0.05 bar(g). The results were obtained using the 100 mm tube and in the previously explained pressure range. To accurately investigate the behaviour of the inner core and potentially describe the mechanism of its formation, it was decided to perform an analysis at two locations: 1/3 (A) and 2/3 (B) of the length of the tube. To obtain further insight, the image light intensity of the visualization was analysed. For the selected region of flow, as illustrated in Fig. 6, the space–time evolution of the light intensity is presented in Fig. 7. The Figure illustrates that the upper and lower boundaries of the inner vortex are not temporally fixed, but rather, their thickness varies over time. Furthermore, it can be noted that the region near the control valve exhibits a significantly higher intensity of the observed variability, as depicted by the dense dark stripes on the plot, which represent the inner jet. Closer to the outlet orifice, the core's instability intensifies, and more erratic behaviour of the core is registered. This observation suggests an increased mixing of the fluid near the inlet nozzles and the outlet orifice. It is of particular importance to note that this variability is primarily related to the movement of the core in relation to the axis of symmetry. Xue et al. [48] also obtained comparable results by examining the behaviour of the core in the cross-section of the vortex tube. The compliance of the inner core behaviour for air and water tests has also been confirmed in this case. This is of particular interest, as studies using air have been considered unpromising and difficult to carry out. Studies using incompressible fluids such as water, are more reliable and easier to conduct. However, in the case of the RHVT, it is difficult to determine the exact cause of the phenomenon, as the stratification of temperature is minimal with the use of an incompressible medium and low inlet pressure. Our studies showed that compressible, gaseous media (air in our case), allow significant results to be achieved in flow visualization. Moreover, this kind of media are the default working factors in vortex tube installations and should be considered as the optimum media for studying the phenomenon.

3.1.2. Vortex observation

Due to the extremely high velocities present within the flow structure of RHVT, it was not possible to observe individual aerosol particles. As a result, the mechanism of formation of this particular flow structure could not be determined. However, as part of the experimental studies using air and an aerosol generator, it was decided to investigate very low inlet pressures at which there was no measurable temperature difference between the hot and cold outlets. As the result, it was possible to observe individual aerosol particles within the flow structure, which exhibited notable vortex-like structures. These structures were identified as alternating vortices, which moved towards the cone-shaped control valve, creating a corridor in the central region of the flow. This resulted in a counter-directional flow of the fluid towards the cold outlet (outlet orifice), this is seen in Fig. 8.

3.2. Water investigation

Initially, an approach similar to the air-based experiments was planned for the water-based research, involving a series of recordings

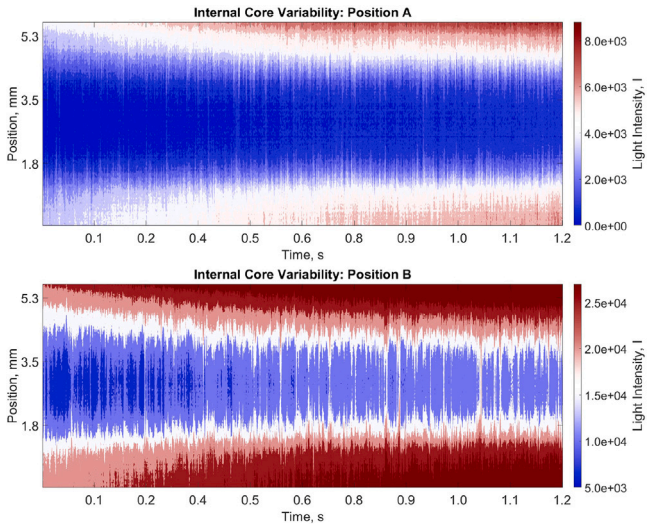

Fig. 7. Recording in 800 fps, $\tau = 1$ to 2,25 s. Top: Spacetime plot of the internal core variability 100 mm tube, location A. Bottom: Spacetime plot of the internal core variability 100 mm tube, location B.

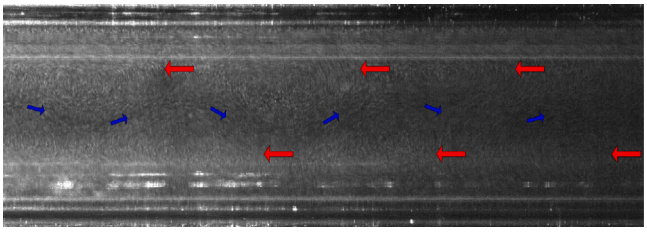

Fig. 8. Alternating vortices (red arrows) and the path they create in the centre of the flow (blue arrows), visible at very low inlet pressure to the RHVT. (For interpretation of the references to colour in this figure legend, the reader is referred to the web version of this article.)

for individual pressure settings and recordings demonstrating a steady increase in pressure. However, due to the observed cavitation, the approach was modified, with a specific focus on areas near the outlet nozzle and the control valve.

3.2.1. Behaviour of the inner core

Similarly as for the air investigations, the inner core is also apparent as a darker region of the flow in the central region of the pipe, as seen in Fig. 9. The observed behaviour of the core is similar to that observed in the air and can be depicted with the help of a space–time plot shown in Fig. 10. The inner core demonstrates variability, visible as a wavy movement. In closer proximity to the outlet orifice, this variability becomes increasingly pronounced. In addition, a zone of increased fluid mixing is observed in the region of the outlet orifice.

3.2.2. Vortex observation

During the system startup, a flow structure highly reminiscent of that described in Section 3.1.2 was observed. Consequently, a decision was made to analyse this behaviour, with a focus on improving the visibility of individual particles. This analysis revealed that, in the case of water, the injection of the working fluid via nozzles tangentially positioned to the vortex chamber (tube) also induces the formation of vortices, as depicted by the red arrows in Fig. 11. This Figure shows the onset of water flow through the RHVT. At the interface of the visible vortex, a fluid path emerges (blue arrows), moving in the opposite direction to the vortices mentioned before. Based on the tube geometry, the velocities of the individual flow elements (the vortices and the inner jet) were calculated. Despite the low inlet pressure, the inner jet velocity reached 1.1 m/s, highlighting the presence of extremely high velocities within the flow structure of the RHVT.

The post-processing of the received data set and subsequent plotting of spacetime plots in the planes marked in Fig. 11 confirmed the existence of the structures mentioned above. The results presented in Fig. 12 show the changes that are occuring in the flow over 1000 frames of the recording.

3.2.3. Cavitation

During the preparation of the experimental setup for the water-based research, gas bubbles were observed accumulating around the inner vortex. It was determined that air was being entrained into the system, leading to the accumulation of air bubbles within the flow. A search for leaks was initiated. The inlet and outlet hoses of the main circulation pump were replaced and the seals of all threaded components were improved using Teflon tape. Upon restarting the system, gas bubbles continued to accumulate around the inner core. Consequently, a more detailed investigation of the observed phenomenon was undertaken. An analysis of the impact of inlet pressure to the RHVT on bubble behaviour was conducted. The results revealed that gas bubbles appeared when the inlet pressure exceeded 0.6 bar(g). Changes in pressure above or below this value resulted in the rapid formation and disappearance of bubbles. Subsequently, it was determined whether air was accumulating in the outlet hoses of the RHVT, which could be drawn into the interior of the RHVT during pump shutdown. In addition, a fluid reservoir was placed above the RHVT to facilitate the removal of any gas bubbles. To completely fill the system with water, the hot outlet of the RHVT was blocked. It was anticipated that this would completely fill the system with water and expel any remaining gas bubbles through the other outlet. Unexpectedly, it was observed that a tornado-like structure appeared within the RHVT shortly after (within a few seconds) of blocking the hot outlet, moving from the hot outlet (regulatory cone) to the cold outlet (orifice). A loud, hissing sound accompanied this observed structure. After further investigation, it was concluded that the observed phenomenon was *cavitation*. Subsequent high-speed camera recordings facilitated the observation of intense cavitation in the form of a tornado-like structure, Fig. 13, as well as the formation and the subsequent disappearance of a gas bubble, Figs. 14 and 15. These phenomena were initially identified in the 180 mm tube. Subsequent testing using other tube lengths (100 and 240 mm) confirmed that cavitation also occurs. Furthermore, the observed behaviour was identical. In the case of the tornado-like structure, its formation was observed in closer proximity to the control valve, after which it moved towards the orifice. After that, the structure stopped its movement and persisted in the flow, approximately 2 cm from the orifice, as shown in Fig. 16. Additionally, during the normal operation of the vortex tube, an audible sound (much weaker and less frequent) was noted, which resembled the bursting of small bubbles in the water. The observed behaviour of the gas bubbles was inconsistent with the expected outcome. As presented in Fig. 17, bubbles were observed to form along the entire length of the pipe, with the majority occurring near the inlet to the device, (a). The bubbles then persisted in the inner flow and moved towards the control cone, where they began to form a chain of single bubbles, (b). As their quantity increased, they merged to form larger bubbles, (c).

4. Discussion

4.1. Related phenomena

The experimental findings presented in Section 3 reveal vortex structures that present a large scale of instabilities and flow oscillations that are well known in fluid mechanics. Before discussing the structures observed in the present investigation, we shall briefly summarize some related phenomena.

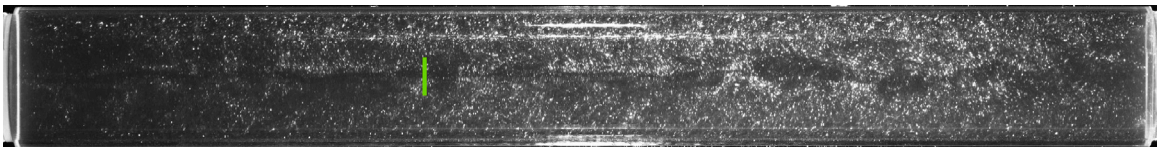

Fig. 9. Visualization of flow in the RHVT using water as working fluid, 180 mm tube, 1,5 bar. The area for post processing is marked as a green line.

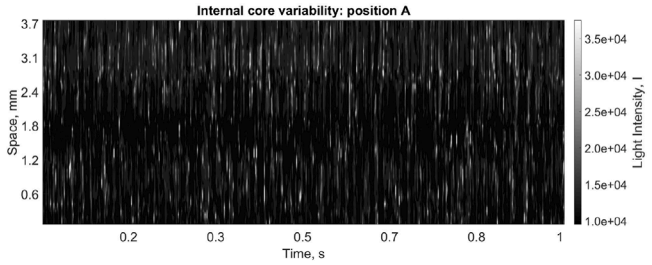

Fig. 10. Water investigation, recording in 600 fps, $\tau = 0$ to 1 s. Post processing for the area marked in Fig. 9. Spacetime plot of the internal core variability 180 mm tube, inlet pressure 1,5 bar.

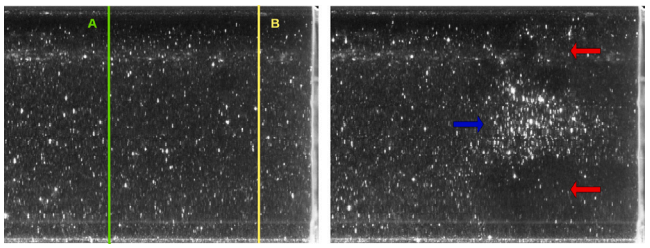

Fig. 11. On the left: reference picture with marked locations for post processing: green - A and yellow - B. On the right: two visible vortices at the beginning of the flow (red arrows) and a suction motion occuring in the centre of the flow (blue arrow). (For interpretation of the references to colour in this figure legend, the reader is referred to the web version of this article.)

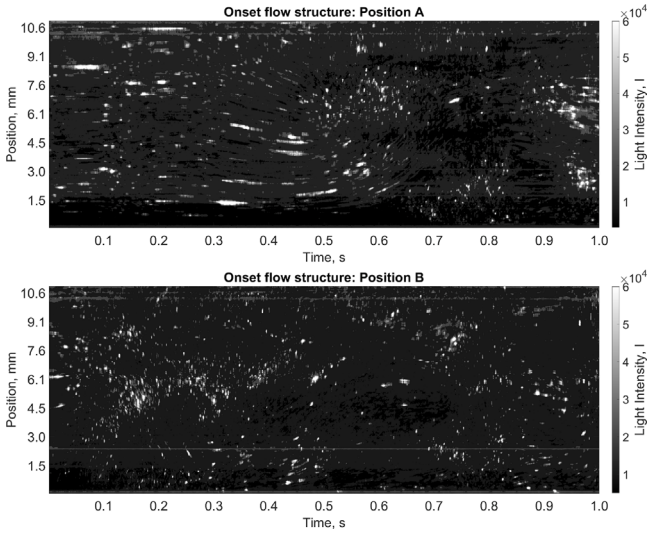

Fig. 12. Water investigation orifice section, recording in 1000 fps, $\tau = 0$ to 1 s. Top: Spacetime plot of the onset of the flow in the 180 mm tube, location A. Bottom: Spacetime plot of the onset of the flow in the 180 mm tube, location B.

The *Kelvin–Helmholtz instability* is a phenomenon that occurs at the interface between fluids of different velocities. It gives rise to small, unstable perturbations, which gradually grow into vortex rolls. Over time, these vortex rolls coalesce to form larger structures [57]. This process enhances mixing and is characterized by a well-defined energy cascade [58].

The second phenomenon is *the von Karman vortex street* is a repeating pattern of vortices occurring when a fluid flows past a cylindrical object, creating alternating low-pressure vortices on either side [59], with regularity and frequency influenced by the fluid inertia, described by the Reynolds number [60]. Vortices exhibit helical symmetry, where the vortex lines spiral around a central axis [61].

The third phenomenon to be delineated is the **toroidal vortices**, which manifests in confined systems. This phenomenon stands in contrast to the previous two, which occur in free space. These vortices are noted for their instability [62] with a tendency to merge into spiral vortices under various conditions. A good example of that is the Taylor–Couette system with axial end walls. In this case toroidal vortices transition into spiral vortices, forming stable wavy spiral structures. This is influenced by the end wall effects, which play a significant role in the transition process [63,64].

4.2. Vortex formation in the RHVT

In the case of the studied RHVT, vortices are constrained by the presence of the pipe wall, preventing their outward movement. Through the observation of the fluid behaviour within the vortex tube, along with an analysis of the established examples of fluid mechanics presented in Section 4.1, it was possible to delineate the formation of the flow structure within the device. The footage from the RHVT water based study shown in Fig. 18 demonstrated that at the onset of the flow, one of the observed vortices, first the upper vortex, exhibited a higher velocity, thereby advancing in front of the lower one. Subsequently, a change in the flow pattern was observed, where the lower vortex began to overtake the upper one. Additionally, a counterflow was observed between the vortices, forming a structure comparable to the inner jet. It is therefore predicted that the observed behaviour causes an instability of the toroidal vortices, resulting in their displacement and subsequent merging into a spiral vortex, which represents the basic flow element in the RHVT (see Fig. 19). This interpretation is further supported by the observed variability of the internal vortex. Subsequently, the liquid progressed towards the hot outlet, where a part of the fluid exited the device. As a consequence of the appearance of a large end–vortex system and a pressure gradient in the vicinity of the cone-shaped control valve, the other part of the fluid was redirected back towards the tube. The inverted portion of the liquid was propelled in the space between the vortices (inner jet) and moved towards the cold outlet (orifice). Studies conducted as part of this research (the use of a cone-shaped regulation valve with an additional 1 mm hole in its axis resulted in air or water flowing out), as well as previous investigations [11], have determined that the pressure at the apex of the cone is higher than the pressure observed at the outlets of the RHVT, where almost atmospheric pressure was measured.

An alternative explanation could involve the presence of a double-helical vortex. In such a scenario, we would expect to observe a substantially greater number of vortices, more closely spaced, than that observed in the experimental investigation.

According to the observed behaviour of the vortices it is also plausible that the main vortex moving along the tube wall may transfer kinetic energy to the inner jet. This hypothesis could explicitly explain the formation of the inner vortex. However, this is difficult to prove via experimental research.

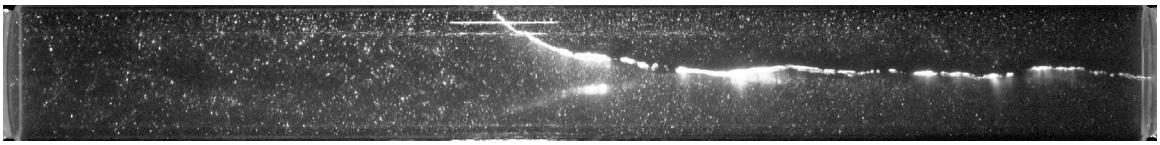

Fig. 13. Tornado-like structure recorded in the 180 mm tube.

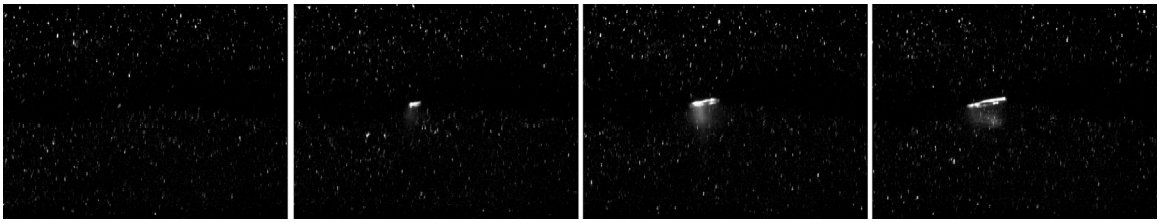

Fig. 14. Formation of a gas bubble, from left to right: $\tau = 0$ to $3.08 \cdot 10^{-4}$ s.

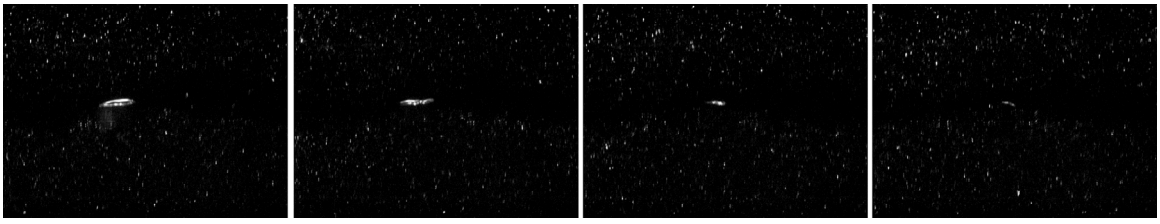

Fig. 15. Disappearance of a gas bubble, from left to right: $\tau = 3.84 \cdot 10^{-4}$ to $6.15 \cdot 10^{-4}$ s.

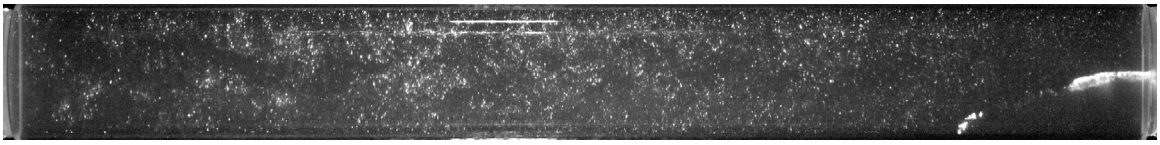

Fig. 16. Persisting tornado-like structure in the orifice/inlet region, intense cavitation.

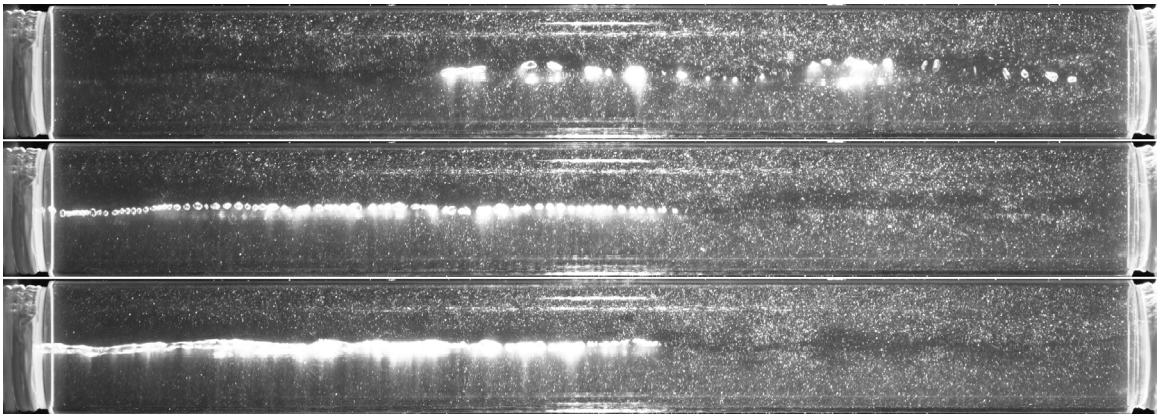

Fig. 17. Movement of the gas bubbles persisting in the centre of flow. From the top: (a) Bubbles occuring and moving towards the regulation valve, (b) Persisting in the inner flow and creating a chain of bubbles, (c) Merging to bigger bubbles.

4.3. Cavitation in the RHVT

The observed cavitation phenomenon in RHVT represents a significant discovery in understanding the underlying causes of the Ranque–Hilsch effect.

Cavitation is the formation of vapour cavities (bubbles) in a liquid – typically water – due to the forces acting upon it, such as a rapid change in pressure. These cavities are created when the local pressure drops below the liquid's vapour pressure, leading to the formation of gas-filled voids. These bubbles can collapse violently, causing significant damage to materials and surfaces, [65]. Cavitation can occur in various environments and systems, including hydraulic machinery, pumps, propellers, and biomedical devices. It is notably prevalent in regions where liquids are subjected to rapid pressure changes, such as the trailing edge of a propeller blade or within a pump impeller. The cavitation mechanism involves the formation, growth, and subsequent collapse of vapour bubbles in a liquid. Initially, small gas pockets serve as the starting point for bubble formation when local pressure drops.

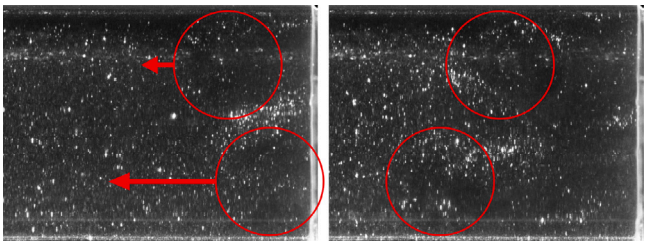

Fig. 18. Behaviour of two visible vortex structures at the beginning of flow in RHVT. See also supplementary material 1.

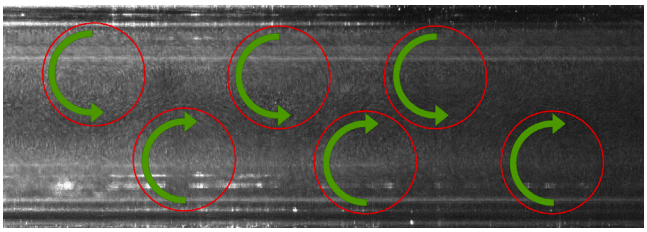

Fig. 19. Alternating vortices wrapping around a wake observed in RHVT. See also supplementary material 2.

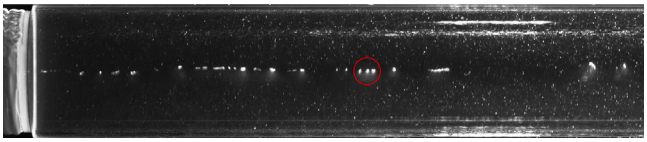

Fig. 20. Gas bubbles persisting in the centre of the flow.

As the pressure decreases further, these bubbles grow and eventually collapse when the pressure is restored [66], this and the characteristic sound appearing was observed in the RHVT during the experimental investigation, Section 3.2.3.

It is interesting to observe that for the applied water temperature range of 22 to 26 °C (depending mainly on the ambient temperature in the laboratory), the saturation pressure ranges from 2.64 to 3.36 kPa. Therefore, the occurrence of this phenomenon directly proves and visualizes the existence of a very low pressure region within the flow of the RHVT.

4.4. Bubble behaviour

The observed behaviour of gas bubbles in experimental studies was a key element of the water investigation. The movement of bubbles around the inner vortex in a direction opposite to the expected flow at this location, and their subsequent accumulation at the control valve, represent a significant research question to be addressed. The proposed explanation is as follows: Due to the high rotational speed and the action of centrifugal forces, the flowing liquid is ejected outwards, resulting in a significant reduction in pressure within the flow, which is confirmed by cavitation, leading to the formation of bubbles.

(i) Bubble persisting in the centre of the flow

The gas bubble formed then became a resistance in the flow, slowing down the surrounding fluid. Due to the rotational nature of the flow, the fluid was ejected outwards, leaving the bubble in the centre of the flow, moving in close proximity to the internal vortex (see Fig. 20).

(ii) Bubble movement along the axis

Due to the bubble acting as a resistance to the flow and the deceleration of the surrounding fluid, the pressure gradient in the immediate vicinity of the bubble decreased. This caused the bubble to move towards the conical regulating valve instead of following the inner vortex flow towards the orifice (cold outlet) (see Fig. 21).

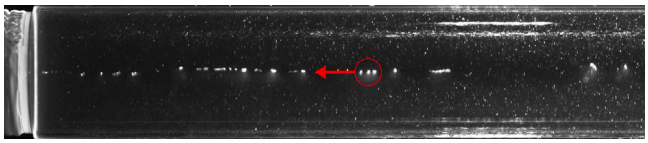

Fig. 21. Gas bubble moving towards the cone-shaped control valve.

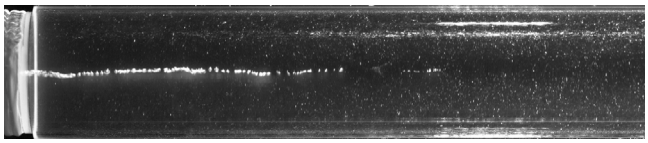

Fig. 22. Gas bubbles accumulating in the regulation valve region.

(iii) Accumulation of the bubbles

Finally, the bubble reached a point where the fluid moving around the bubble towards the cold outlet accelerated it at the same rate as the movement caused by the pressure gradient towards the conical regulating valve. As a result, the bubbles began to accumulate and persist in this region, forming a chain of separate bubbles. The bubbles did not merge due to surface tension. After a while, the bubbles were observed to merge when their number became large enough to overcome the surface tension (see Fig. 22).

4.5. Working principle hypothesis

The observations and conclusions obtained from the RHVT flow structure studies, and in particular the observed cavitation, have led to the formulation of two additional hypotheses to further elucidate the underlying physics of the phenomenon. The first one described as **Gas humidity** was a temporary working hypothesis discontinued after further literature analysis. It was based on the water visualization experiments, where the low pressure region within the vortex tube was observed. The idea behind this hypothesis was that according to the ideal gas law a decrease in pressure under conditions of constant volume and gas quantity results in a corresponding temperature drop. In addition, it can be assumed that most gases (including atmospheric air) contain a certain amount of moisture. If the pressure in the vicinity of the internal vortex is close to vacuum, the water immediately begins to boil, even at low temperatures. This was observed in the water investigation in the form of cavitation. For the case of humid air a decrease in pressure entails the decrease of the saturation temperature. As a result, with further pressure reduction, the previously condensed droplets may also begin to boil and expand rapidly in the low pressure region. This phase transition will result in heat absorption from the internal vortex. Subsequently, because of its rapid expansion, the vapour will reach a higher pressure region — the border between the inner and outer flow. As the pressure increases, the water vapour formed under vacuum conditions may now recondense because the higher pressure can support the liquid phase again. Eventually, the water or moisture in the air reaches a new equilibrium where the liquid and gaseous phases coexist according to the ambient temperature and the new pressure conditions. Because of the centrifugal force, the water is then pushed further outward, to a zone with an even higher pressure. Due to the increase in pressure, it will start to evaporate again because of the rising temperature. This process adds water vapour back into the air, increasing the humidity. After reaching the cone-shaped regulation valve area, part of the humid gas will be redirected into the inner flow, and the whole process will repeat, establishing a process similar to a Rankine cycle, and explaining why temperature stratification occurs.

Although at first this hypothesis seemed to be reasonable, literature data and observations have proven it to be invalid. Firstly, the amount of water in the air is not significant. For example, at a temperature of 300 K and a relative humidity of 50%, the moisture content would be approximately 0.012 kg H_2O/kg dry air. Secondly, assuming that this hypothesis describes the primary mechanism of heat transport in RHVT, the effect should not occur or should be significantly weaker in dry gases. However, the literature provides information about experiments with gases such as N_2, CO_2, and He, where in all cases the authors report the occurrence of the phenomenon [67–70].

The second hypothesis that can be derived is referred to as the "centrifugal compressor hypothesis". This hypothesis is regarded as the most plausible explanation for the physics of the phenomenon, as determined by the observations made in this experimental study. The majority of hypotheses concerning the Ranque–Hilsch phenomenon attempt to identify the underlying cause of temperature stratification with a mechanism analogous to that observed in heat pumps. However, it is plausible that the explanation of the phenomenon is more straightforward, and that the mechanism of gas compression itself, through the action of centrifugal force and volume change (a property of a compressible fluid), is responsible for this temperature difference. The results of experimental studies indicate that the compressibility of the working medium greatly influences the phenomenon. It has been observed in various gases (air, CO_2, helium, etc. compressible fluids), but in water (incompressible fluid), the majority of literature sources indicate that the phenomenon does not occur, [47,48]. Similar observations were made in this study. Other reported observations show the following relationships:

i For the given valve setting, increasing the inlet pressure increases the temperature difference;
ii For the given inlet pressure, opening the valve results in a decrease of the cold outlet temperature and also a decrease of the hot outlet temperature to a point after which the main flow will start sucking in air through the orifice, similar to an ejector;
iii Increasing the length of the tube results in an increase of the temperature difference, until a certain critical length is reached. Further length increment results in the deterioration of the effect;
iv For a closed regulation valve (only the cold-end outlet active), the outlet temperature constantly and slowly increases with time;
v Prior numerical studies within the ATHLETE project, based on elementary energy equations have demonstrated a temperature separation in both dry and humid gases, without incorporating phase change modelling;

The conclusions drawn from previous studies of the phenomenon did not allow to point out a specific mechanism that could directly influence the observed temperature difference. Therefore, it is conceivable that the operation of a vortex tube can be explained similarly to the model proposed by Georges Ranque, who postulated adiabatic expansion in the core and adiabatic compression in the outer layer. The hypothesis presented in this section, assumes that the centrifugal force alone is sufficient to create a centrifugal compressor effect within the vortex tube, an effect which is amplified by the presence of a very low-pressure region in the tube's interior. According to this hypothesis, there is no need to postulate the existence of a specific mechanism that would enable a 'heat pump' cycle.

Consider three layers of fluid: A, B, and C as shown in Fig. 23. Assuming a fixed co-ordinate system applied to the vortex tube axis, and assuming that the tangential velocity $v_t = \omega r$ is the dominating component of the velocity vector, one can note that the layer B can only be maintained in rotation by the *centripetal* force, resulting from the difference in pressures of layers A and C:

$$\omega^2 r \, \mathrm{d}m = S \, \mathrm{d}p, \tag{3}$$

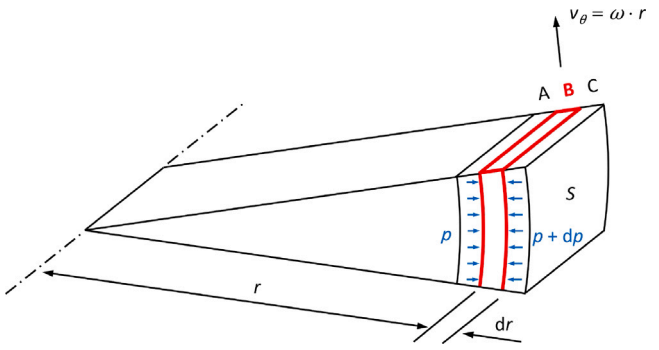

Fig. 23. Pressure field in the rotating fluid.

Table 2
Sample results of radial pressure distribution in a centrifugal field from data based on water, low pressure air and high pressure air experiments.

Parameter	Value		
	Water	Air	
Radius, m		0.006	
Inlet pressure (experimental), kPa	575	118	700
Tangential velocity, m/s	28.3	91.6	237
Angular velocity, rad/s	4722.2	15 267	39 500
Isentropic exponent	–	1.4	1.4
Temperature in the core, K	293	292	267
Temperature at the outer wall, K	293	296.2	294.8
Pressure in the core, kPa	1.5	100	100
Pressure at the outer wall, kPa	403	105.1	141.5

where S is a surface of the fluid element B perpendicular to the plane of analysis. Neglecting the variability of S one can obtain:

$$\mathrm{d}p = \rho\omega^2 r \, \mathrm{d}r \tag{4}$$

For incompressible fluids, the following radial pressure distribution can be derived:

$$p(r) = p_0 + \frac{\rho\omega^2 r^2}{2} \tag{5}$$

For gases (compressible fluids), one has to account for the equation of state (EoS), as well as for the temperature–pressure dependency during compression. Assuming the ideal gas EoS and an isentropic compression one can write:

$$\rho = \frac{p}{RT} \quad \text{and} \quad \left(\frac{p}{p_0}\right)^{\frac{\kappa-1}{\kappa}} = \frac{T}{T_0} \tag{6}$$

Substituting these equations into Eq. (4) and performing the required integration, the following pressure distribution is obtained:

$$p = p_0 \left(1 + \frac{\kappa - 1}{2\kappa} \frac{\omega^2 r^2}{RT_0}\right)^{\frac{\kappa}{\kappa-1}} \tag{7}$$

Based on the derived equations and fluid velocities obtained from the experimental data, the following pressure and temperature distribution in a theoretic 1D pressure field is obtained (Table 2).

As it can be seen, the impact of the centrifugal/centripetal forces on the pressure temperature differs substantially between the considered fluids. For water, there is no temperature increment due to the pressure gradient, while the pressure gradient is very high despite a lower angular velocity. On the contrary, for air the pressure gradient created by the rotation of the fluid is less pronounced even for high inlet pressure and velocity; at the same time, this gradient creates a significant temperature increment. This increment is still noticeable for low inlet pressures and moderate velocity and its value is in agreement with the experimentally observed values described in Section 2.1.1.

While the presented considerations are idealized and based on a one-dimensional radial formulation and the ideal gas, adiabatic expansion, they suffice to detect the fundamental thermodynamic laws governing the flow physics in the studied vortex tube.

5. Conclusions

At the current state of knowledge, the reasons for the occurrence of the Ranque–Hilsch phenomenon still remains unclear. The high rotational and linear velocities present in the flow made it challenging to obtain the anticipated measurement outcomes. In the case of tests using aerosol, it was not possible to visualize the individual aerosol particles, which burst due to the excessive pressure, resulting in flow disturbances and visible condensation. The use of water facilitated a better observation of the flow structure; however, the Ranque–Hilsch phenomenon was not occurring in this case (no temperature difference). Furthermore, comparing the results obtained in compressible and incompressible liquids also presents a number of problems associated with significant differences in their physical properties. However, a number of conclusions could be drawn directly from the experimental studies conducted:

1. The observed structure within the interior of the flow, as depicted in the visualization studies, represents the internal flow structure of the RHVT. The formation of this structure is primarily attributed to the pressure gradient that is generated in the vicinity of the control cone. This was observed as a growth of the structure going from the regulation cone to the outlet orifice. Furthermore, it is expected, that the transfer of kinetic energy from the outer vortex flow to the inner jet also plays a significant role, Section 3.
2. The analysis of the behaviour of the internal vortex demonstrated the feasibility of experimental studies using air as a working fluid. The obtained results are consistent with the reported literature for water, and add novel value for air flow visualization.
3. The vortices observed during the study are anticipated to be toroidal vortices, and because of their inner instability they begin to overlap and consequently form a spiral vortex that underlies the main flow in the vortex tube and whose velocity increases as the inlet pressure increases.
4. The observation of the occuring cavitation and the subsequent analysis of the behaviour of the bubbles enabled the description of the low-pressure region occurring inside the flow, Section 4.3.
5. The radial pressure field is more pronounced for liquids due to higher inertia forces, on the other hand, it contributes to the R-H effect in gases at least partially, due to the temperature-pressure dependency in the compression process. The R-H effect may be amplified by other phenomena, as discussed in the literature review.
6. The observed flow structure and cavitation provide a valuable basis for further numerical modelling and achieving a fully validated numerical model in agreement with both global and local flow conditions.

In addition, it is important to emphasize the significance of the observed cavitation. With this discovery, the RHVT can become an effective tool for further research on the cavitation process. Cavitation is a critical area of research due to its dual nature: it can be both detrimental and beneficial depending on the context. On the one hand, cavitation causes wear and damage to hydraulic machinery, posing a significant challenge for engineering and design. Understanding cavitation wear is essential for selecting appropriate materials and optimizing system design to mitigate these adverse effects [71]. On the other hand, cavitation has promising applications in fields like biomedical engineering, where it is applicable for therapeutic purposes [72]. This potential for both harmful effects to be avoided and possible beneficial applications makes cavitation an interesting topic of further research.

6. Outlook

The objective of the experimental study presented in this work was to investigate the flow structure inside a Ranque–Hilsch vortex tube. The observed behaviour of the inner vortex and the cavitation occurring around the inner core are the phenomena that can be modelled within the planned numerical studies. Agreement between experimental and numerical studies is essential to enable the investigation of a broader range of settings and direct observations of the device's internal dynamics.

While the presented pressure/temperature dependency provides a reasonable explanation of the primary thermal separation mechanism, the energy-based explanation of the effect and the impact of secondary mechanisms should be investigated more thoroughly in future work. Among them, one should emphasize on the potential influence of acoustics. The acoustic hypothesis has yet to be fully explored, and it shows promising potential for further research.

CRediT authorship contribution statement

Marcel Barzantny: Writing – review & editing, Writing – original draft, Visualization, Software, Methodology, Investigation, Formal analysis, Data curation, Conceptualization. **Mohammed Hussein Hamede:** Writing – review & editing, Writing – original draft, Visualization, Supervision, Resources, Methodology, Investigation, Formal analysis, Conceptualization. **Michał Majchrzyk:** Writing – review & editing, Writing – original draft, Validation, Software, Methodology, Conceptualization. **Sebastian Merbold:** Writing – review & editing, Visualization, Supervision, Software, Methodology, Investigation, Conceptualization. **Christoph Egbers:** Writing – review & editing, Supervision, Resources, Funding acquisition, Conceptualization. **Wojciech Kostowski:** Writing – review & editing, Writing – original draft, Visualization, Supervision, Project administration, Methodology, Investigation, Funding acquisition, Formal analysis, Conceptualization.

Declaration of competing interest

The authors declare that they have no known competing financial interests or personal relationships that could have appeared to influence the work reported in this paper.

Acknowledgements

This research work was possible thanks to the support of the National Science Centre of Poland, which financed the research project NCN-Opus nr 2021/43/B/ST8/03320 (UMO-2021/43/B/ST8/03320) 'ATHLETE' and the ERASMUS+ program, which made it possible to carry out experimental studies in the facilities of the Brandenburg University of Technology.

The authors would also like to thank the ATHLETE project team for their support, and the whole team at Dept. of Aerodynamics and Fluid Mechanics at Brandenburg University of Technology CS for their constant support in the laboratory.

Appendix A. Supplementary data

Supplementary material related to this article can be found online at https://doi.org/10.1016/j.ijheatmasstransfer.2025.127543.

Data availability

Data will be made available on request.

References

[1] G. Ranque, et al., Experiments on expansion in a vortex with simultaneous exhaust of hot air and cold air, J. Phys. Radium 4 (7) (1933) 112–114.

[2] B.M. Mendecka, D. Chiappini, G. Bella, Cooling Performance of an Modified R744 Air Conditioning System with Vortex Tube and Internal Heat Exchanger for an Electric Vehicle, Tech. rep., SAE Technical Paper, 2021.

[3] W. Wang, J. Wang, Y. Wu, X. Liu, Analysis of energy separation mechanism of vortex tube and collaborative study with cold end aperture based on inlet nozzle diameter, Int. J. Heat Fluid Flow 115 (2025) 109865, http://dx.doi.org/10.1016/j.ijheatfluidflow.2025.109865, URL https://www.sciencedirect.com/science/article/pii/S0142727X25001237.

[4] V. Alekhin, V. Bianco, A. Khait, A. Noskov, Numerical investigation of a double-circuit Ranque–Hilsch vortex tube, Int. J. Therm. Sci. 89 (2015) 272–282.

[5] V. Bianco, A. Khait, A. Noskov, V. Alekhin, A comparison of the application of RSM and LES turbulence models in the numerical simulation of thermal and flow patterns in a double-circuit Ranque-Hilsch vortex tube, Appl. Therm. Eng. 106 (2016) 1244–1256.

[6] A. Khait, A. Noskov, V. Alekhin, V. Bianco, Analysis of the local entropy generation in a double-circuit vortex tube, Appl. Therm. Eng. 130 (2018) 1391–1403.

[7] S.E. Rafiee, M. Sadeghiazad, Three-dimensional numerical investigation of the separation process in a vortex tube at different operating conditions, J. Mar. Sci. Appl. 15 (2016) 157–165.

[8] T. Amitani, T. Adachi, T. Kato, A study on temperature separation in a large vortex tube, JSME Trans. 49 (440B) (1983) 877–884.

[9] W. Lewellen, A solution for three-dimensional vortex flows with strong circulation, J. Fluid Mech. 14 (3) (1962) 420–432.

[10] D. Schlenz, Kompressible Strahlgetriebene Drallstrohmung in. rotationssymmetrischen Kanalen (Ph. D. Thesis), Univ. Erlangen, 1982.

[11] P. Bargiel, J. Skorek, S. Usón, A. Klimanek, W. Kostowski, Vortex tube operational temperature regime, J. Energy Resour. Technol. 142 (8) (2020) 082001.

[12] B. Ahlborn, S. Groves, Secondary flow in a vortex tube, Fluid Dyn. Res. 21 (2) (1997) 73–86, http://dx.doi.org/10.1016/S0169-5983(97)00003-8, URL https://www.sciencedirect.com/science/article/pii/S0169598397000038.

[13] Y. Xue, M. Arjomandi, R. Kelso, A critical review of temperature separation in a vortex tube, Exp. Therm. Fluid Sci. 34 (8) (2010) 1367–1374.

[14] B. Ahlborn, S. Groves, Secondary flow in a vortex tube, Fluid Dyn. Res. 21 (2) (1997) 73.

[15] B.K. Ahlborn, J.M. Gordon, The vortex tube as a classic thermodynamic refrigeration cycle, J. Appl. Phys. 88 (6) (2000) 3645–3653.

[16] T. Cockerill, Thermodynamics and fluid mechanics of a Ranque-Hilsch vortex tube, Univ. Camb. (1998).

[17] C. Gao, K. Bosschaart, J. Zeegers, A. De Waele, Experimental study on a simple Ranque–Hilsch vortex tube, Cryogenics 45 (3) (2005) 173–183.

[18] F. Schultz-Grunow, Turbulenter wärmedurchgang im zentrifugalfeld, Forsch. Auf Dem Geb. Ingenieurwesens A 17 (1951) 65–76.

[19] K. Stephan, S. Lin, M. Durst, F. Huang, D. Seher, An investigation of energy separation in a vortex tube, Int. J. Heat Mass Transfer 26 (3) (1983) 341–348.

[20] D. Webster, An analysis of the Hilsch vortex tube, Refrig. Eng. 58 (2) (1950) 163.

[21] R. Deissler, M. Perlmutter, Analysis of the flow and energy separation in a turbulent vortex, Int. J. Heat Mass Transfer 1 (2–3) (1960) 173–191.

[22] A. Gutsol, The ranque effect, Phys.-Usp. 40 (6) (1997) 639.

[23] O. Kazantseva, S.A. Piralishvili, A. Fuzeeva, Numerical simulation of swirling flows in vortex tubes, High Temp. 43 (4) (2005) 608–613.

[24] C. Linderstrm-Lang, The three-dimensional distributions of tangential velocity and total-temperature in vortex tubes, J. Fluid Mech. 45 (1) (1971) 161–187.

[25] C.D. Pengelley, Flow in a viscous vortex, J. Appl. Phys. 28 (1) (1957) 86–92.

[26] A. Hamoudi, A. Fartaj, G. Rankin, Performance characteristics of a microscale Ranque–Hilsch vortex tube, 2008.

[27] N. Bej, K. Sinhamahapatra, Numerical analysis on the heat and work transfer due to shear in a hot cascade Ranque–Hilsch vortex tube, Int. J. Refrig. 68 (2016) 161–176, http://dx.doi.org/10.1016/j.ijrefrig.2016.04.021, URL https://www.sciencedirect.com/science/article/pii/S0140700716300731.

[28] R. Hilsch, Die expansion von gasen im zentrifugalfeld als kälteprozess, Z. Nat.forsch. A 1 (4) (1946) 208–214.

[29] U. Behera, P. Paul, K. Dinesh, S. Jacob, Numerical investigations on flow behaviour and energy separation in Ranque–Hilsch vortex tube, Int. J. Heat Mass Transfer 51 (25–26) (2008) 6077–6089.

[30] T. Farouk, B. Farouk, Large eddy simulations of the flow field and temperature separation in the Ranque–Hilsch vortex tube, Int. J. Heat Mass Transfer 50 (23–24) (2007) 4724–4735.

[31] T. Farouk, B. Farouk, A. Gutsol, Simulation of gas species and temperature separation in the counter-flow Ranque–Hilsch vortex tube using the large eddy simulation technique, Int. J. Heat Mass Transfer 52 (13–14) (2009) 3320–3333.

[32] A. Secchiaroli, R. Ricci, S. Montelpare, V. D'alessandro, Numerical simulation of turbulent flow in a Ranque–Hilsch vortex tube, Int. J. Heat Mass Transfer 52 (23–24) (2009) 5496–5511.

[33] M. Kurosaka, Acoustic streaming in swirling flow and the Ranque—Hilsch (vortex-tube) effect, J. Fluid Mech. 124 (1982) 139–172.

[34] J.Q. Chu, Acoustic Streaming as a Mechanism of the Ranque-Hilsch Effect, The University of Tennessee, 1982.

[35] A. Kaufmann, Ranque Hilsch Vortex Tube Demystified, Springer, 2022.

[36] S. Syed, M. Renganathan, Numerical investigations on flow characteristics and energy separation in a Ranque Hilsch vortex tube with hydrogen as working medium, Int. J. Hydrog. Energy 44 (51) (2019) 27825–27842.

[37] S.E. Rafiee, M. Sadeghiazad, Experimental and 3D CFD analysis on optimization of geometrical parameters of parallel vortex tube cyclone separator, Aerosp. Sci. Technol. 63 (2017) 110–122.

[38] X. Guo, B. Liu, J. Lv, B. Zhang, Y. Shan, An optimization method on managing Ranque–Hilsch vortex tube with the synergy between flow structure and performance, Int. J. Refrig. 126 (2021) 123–132, http://dx.doi.org/10.1016/j.ijrefrig.2020.12.031, URL https://www.sciencedirect.com/science/article/pii/S0140700720305259.

[39] K. Shaji, K.-K. Lee, F. Salmani, H.D. Kim, Numerical analysis and an approach for optimization of the Ranque–Hilsch vortex tube for a compressible flow, Appl. Therm. Eng. 243 (2024) 122590, http://dx.doi.org/10.1016/j.applthermaleng.2024.122590, URL https://www.sciencedirect.com/science/article/pii/S1359431124002588.

[40] R. MacGee Jr., Fluid action in the vortex tube, J. ASRE Refrig. Eng. 58 (1950) 974–975.

[41] P. Baker, Investigations on the Ranque-Hilsch (Vortex) Tube, Oak Ridge National Laboratory, 1954.

[42] J. Lay, An experimental and analytical study of vortex-flow temperature separation by superposition of spiral and axial flow: part 2, J. Heat Transf. 81 (3) (1959) 213–221.

[43] M. Sibulkin, Unsteady, viscous, circular flow part 3. application to the Ranque-Hilsch vortex tube, J. Fluid Mech. 12 (2) (1962) 269–293.

[44] V. Arbuzov, Y.N. Dubnishchev, A. Lebedev, M.K. Pravdina, N. Yavorski, Observation of large-scale hydrodynamic structures in a vortex tube and the Ranque effect, Tech. Phys. Lett. 23 (1997) 938–940.

[45] O. Aydın, M. Baki, An experimental study on the design parameters of a counterflow vortex tube, Energy 31 (14) (2006) 2763–2772.

[46] X. wei Li, H. Yan, J. an Meng, Z. xin Li, Visualization of longitudinal vortex flow in an enhanced heat transfer tube, Exp. Therm. Fluid Sci. 31 (6) (2007) 601–608, http://dx.doi.org/10.1016/j.expthermflusci.2006.06.007, URL https://www.sciencedirect.com/science/article/pii/S0894177706000963.

[47] Y. Xue, M. Arjomandi, R. Kelso, Visualization of the flow structure in a vortex tube, Exp. Therm. Fluid Sci. 35 (8) (2011) 1514–1521.

[48] Y. Xue, J.R. Binns, M. Arjomandi, H. Yan, Experimental investigation of the flow characteristics within a vortex tube with different configurations, Int. J. Heat Fluid Flow 75 (2019) 195–208.

[49] X. Guo, B. Zhang, L. Li, B. Liu, T. Fu, Experimental investigation of flow structure and energy separation of Ranque–Hilsch vortex tube with LDV measurement, Int. J. Refrig. 101 (2019) 106–116, http://dx.doi.org/10.1016/j.ijrefrig.2019.02.004, URL https://www.sciencedirect.com/science/article/pii/S0140700719300544.

[50] Z. Shi, X. Guo, B. Zhang, T. Fu, Large-scale flow structure and energy separation in a Ranque–Hilsch vortex tube with particle image velocimetry measurement: an experimental study, J. Vis. 26 (1) (2023) 45–59.

[51] W. Kostowski, P. Bargiel, M. Barzantny, D. Adamecki, M. Majchrzyk, B. Mendecka, E. Maciak, Experimental setup design for multi-purpose Ranque-Hilsch vortex tube investigation, in: 36th International Conference on Efficiency, Cost, Optimization, Simulation and Environmental Impact of Energy Systems, ECOS 2023, Curran Associates, Inc., 2023, pp. 781–791, http://dx.doi.org/10.52202/069564-0071.

[52] U. Behera, P. Paul, S. Kasthurirengan, R. Karunanithi, S. Ram, K. Dinesh, S. Jacob, CFD analysis and experimental investigations towards optimizing the parameters of Ranque–Hilsch vortex tube, Int. J. Heat Mass Transfer 48 (10) (2005) 1961–1973.

[53] M. Barzantny, M.H. Hamede, S. Merbold, C. Egbers, M. Majchrzyk, W. Kostowski, The Ranque Hilsch phenomenon: Experimental visualization of the flow structure, in: Proceedings of the German Association for Laser Anemometry, GALA e.V., GALA e.V., Karlsruhe, Germany, 2024.

[54] S. Merbold, M.H. Hamede, A. Froitzheim, C. Egbers, Flow regimes in a very wide-gap Taylor–Couette flow with counter-rotating cylinders, Phil. Trans. R. Soc. A 381 (2246) (2023) 20220113.

[55] M.H. Hamede, S. Merbold, C. Egbers, Experimental method for investigating the formation of flow patterns in a very wide gap taylor-couette flow (η=0.1), Tm - Tech. Mess. 90 (5) (2023).

[56] N. Abcha, N. Latrache, F. Dumouchel, I. Mutabazi, Qualitative relation between reflected light intensity by Kalliroscope flakes and velocity field in the Couette–Taylor flow system, Exp. Fluids 45 (2008) 85–94.

[57] T.W.I. Kuan, J. Szmelter, F. Cocetta, LES and ILES simulations of free-jets, Flow Turbul. Combust. 110 (3) (2023) 547–579.

[58] P. Drazin, Kelvin–Helmholtz instability of finite amplitude, J. Fluid Mech. 42 (2) (1970) 321–335.

[59] J. Wagner, Wikimedia commons, 2014, https://commons.wikimedia.org/wiki/File:Karmansche_Wirbelstr_kleine_Re.JPG, (Accessed 20 March 2025).

[60] N. Ohkura, H. Hayafuji, M. Okude, Axial flow in a vortex in Karman vortex street, J. Japan Soc. Aeronaut. Space Sci. 44 (505) (1996) 105–111, http://dx.doi.org/10.2322/jjsass1969.44.105.
[61] C.M. Velte, M.O. Hansen, V.L. Okulov, Helical structure of longitudinal vortices embedded in turbulent wall-bounded flow, J. Fluid Mech. 619 (2009) 167–177.
[62] J.O. Hirschfelder, The angular momentum, creation, and significance of quantized vortices, J. Chem. Phys. 67 (12) (1977) 5477–5483.
[63] S. Altmeyer, C. Hoffmann, M. Heise, J. Abshagen, A. Pinter, M. Lücke, G. Pfister, End wall effects on the transitions between Taylor vortices and spiral vortices, Phys. Rev. E 81 (2010) 066313, http://dx.doi.org/10.1103/PhysRevE.81.066313.
[64] M.H. Hamede, S. Merbold, C. Egbers, Experimental investigation of turbulent counter-rotating Taylor–Couette flows for radius ratio $\eta = 0.1$, J. Fluid Mech. 964 (2023) A36.
[65] A. Acosta, B. Parkin, Cavitation inception—a selective review, J. Ship Res. 19 (04) (1975) 193–205.
[66] Y. Tsujimoto, H. Horiguchi, K. Yonezawa, Flow instabilities in cavitating and non-cavitating pumps, Des. Anal. High Speed Pumps (2006) 7-1–7-24.
[67] G. Jain, A. Arora, S. Gupta, Performance analysis of a transcritical N2O refrigeration cycle with vortex tube, Int. J. Ambient Energy 40 (4) (2019) 350–356.
[68] S. Mohammadi, F. Farhadi, Experimental and numerical study of the gas–gas separation efficiency in a Ranque–Hilsch vortex tube, Sep. Purif. Technol. 138 (2014) 177–185.
[69] J. Yun, Y. Kim, S. Yu, Feasibility study of carbon dioxide separation from gas mixture by vortex tube, Int. J. Heat Mass Transfer 126 (2018) 353–361.
[70] A. Alsaghir, M.O. Hamdan, M.F. Orhan, Fluid properties impact on energy separation in Ranque–Hilsch vortex tube, SN Appl. Sci. 4 (8) (2022) 227.
[71] W. Borek, T. Tański, M. Król, Introductory chapter: Cavitation - an overview of new research results, in: W. Borek, T. Tański, M. Król (Eds.), Cavitation, IntechOpen, Rijeka, 2018, http://dx.doi.org/10.5772/intechopen.81956, Ch. 1.
[72] M. Ghorbani, O. Oral, S. Ekici, D. Gozuacik, A. Koşar, Review on lithotripsy and cavitation in urinary stone therapy, IEEE Rev. Biomed. Eng. 9 (2016) 264–283, http://dx.doi.org/10.1109/RBME.2016.2573381.